Thermo-hydro-mechanical behaviour of deep Ypresian clays

Núria Sau[1,2#], *Enrique* Romero[1,2], and *Hervé* Van Baelen[3]

[1]*CIMNE, Geomechanics Group, Barcelona, Spain*
[2]*UPC, Department of Civil and Environmental Engineering, Barcelona, Spain*
[3]*ONDRAF/NIRAS, R&D-department, Brussels, Belgium*
[#]*Corresponding author: nuria.sau@upc.edu*

ABSTRACT

Investigating the thermo-hydro-mechanical behaviour of deep Ypresian clays (300 to 400 m below ground) is crucial since they are one of Belgium's potential host rock formations for deep geological disposal of radioactive waste. To this aim, a newly designed and fully instrumented thermal oedometer cell with lateral stress measurement was used to determine the stress state accurately. First, well-preserved core samples were loaded to bring them to the large *in situ* stresses and reduce the induced matric suction on deep water-undrained sampling. The remaining matric suction was then reduced by soaking with synthetic water of the formation. Next, drained loading and unloading paths were followed to attain different vertical effective stresses at varying overconsolidation ratios (*OCRs*) before the drained thermal paths (heating and cooling). The results indicated a systematic increase in the horizontal effective stress on heating at constant vertical effective stress. In addition, thermal-induced volume changes in heating/cooling at different *OCRs* were studied. Test results were finally interpreted within a thermo-mechanical elastoplastic framework.

Keywords: deep clay, thermo-hydro-mechanical behaviour, oedometer, temperature.

1. Introduction

The study of the coupled thermo-hydro-mechanical (THM) behaviour of soils and rocks has regained relevance because of the rise in new energy geomechanics applications, particularly in the design of energy geo-structures and energy geo-storage (e.g., (Loveridge et al. 2020)).

More specifically, the present study is framed within the deep geological storage of heat-emitting and long-lived radioactive waste, in which a series of superimposed natural and artificial barriers achieve safe containment of the radionuclides. The natural barrier is the host rock formation, which requires adequate characterisation of the coupled THM processes during the disposal repository's working life. One of Belgium's potential argillaceous host rocks is the deep Ypresian clays (Ycs) formation (300 to 400 m below ground). Therefore, laboratory tests on well-preserved samples at different depths and well-controlled boundary conditions are essential for this formation to overcome the lack of *in situ* tests due to the large depths. For example, (Romero et al. 2016) studied the thermal conductivity of this deep Eocene clay formation with direct measurements and back-analysis results following well-controlled pre-conditioning protocols to ensure the closure of fissures along bedding planes.

Since the late 80s, several authors have addressed the impact of temperature on the volume change and the shear strength response of deep clays (e.g., (Hueckel and Baldi 1990; Delage, Sultan, and Cui 2000)). Particularly, experimental studies have been focused on identifying temperature effects on the preconsolidation stress and consequences of the overconsolidation ratio (*OCR)* on the thermal-induced volume changes (e.g., (Sultan, Delage, and Cui 2002; Laloui and Cekerevac 2003)). Experimental results have shown that the elastic domain shrinks as temperature increases (thermal softening) and that the compressibility and shear strength parameters remain approximately unaffected by temperature. Nevertheless, some aspects should still be investigated. For example, to the authors' knowledge, there are no experimental studies concerning the evolution of radial stresses during drained thermal paths under oedometer conditions. This information would allow a better-defined stress state while accurately measuring volume changes.

This paper describes a new fully instrumented and temperature-controlled oedometer cell prepared for high stresses, allowing local pore pressure monitoring and radial stress measurement with a localised thin-wall system. Pre-conditioning protocols on well-preserved core samples were followed to bring them to the large *in situ* stresses and cancel the induced matric suction on deep water-undrained retrieval by soaking them with synthetic water of the formation. The cell allowed exploring the evolution of the radial stresses along different THM stress paths and further studying the thermal-induced volume changes on drained heating and cooling at constant vertical effective stresses and varying *OCRs*.

2. Material under study

The Eocene Ycs (300 to 400 m below ground) are a relatively thick sequence of dominantly fine-grained marine sediments deposited during the Ypresian Age (55 to 49 Ma). They are slightly overconsolidated, with a yield stress ratio (*YSR)* between 1.2 and 1.8 (Lima 2011; Nguyen et al. 2014; Sau 2021).

Table 1 summarises the main soil properties and the initial state of the two samples tested in the present study. They were carefully retrieved at different depths at Kallo (Belgium) and belonged to distinct lithological units. The sample Core-48 belongs to the silty clay unit called Roubaix. The deeper sample, Core-103, was retrieved from the moderate-hard clay unit Lower Orchies. The mineralogical analyses revealed a quite similar qualitative composition despite the different units. The non-clayey fraction of Core-48 and Core-103 (52 and 47% in bulk, respectively) is mainly constituted by quartz (35 and 33%), alkali feldspar (3 and 5%) and plagioclase (5 and 3%). The clayey fraction (49 and 53% in bulk) is mainly constituted by smectite (21 and 18%), randomly interstratified illite/smectite (14 and 16%) and illite (4 and 7%).

The high initial values of total suction are associated with the large matric suction induced on water-undrained unloading upon retrieval. However, the largest pore sizes detected on Ycs samples (typically around 0.76 to 1.9 µm) cannot sustain such high induced matric suction (Sau, Romero, and Van Baelen 2020). Consequently, some air is expected to invade the soil upon sampling, which induces some slight swelling and desaturation of the material. Moreover, it appears that some drying also occurred during storage.

Table 1. Properties and the initial state of the tested samples.

	Core-48 (335 m)	**Core-103 (390 m)**
Bulk density, ρ (Mg/m^3)	1.96	2.10
Density of solids, ρ_s (Mg/m^3)	2.72	2.73
Water content, w (%)	22.4	18.4
Void ratio, e (-)	0.701	0.540
Degree of saturation, S_r (%)	87.1	92.8
Initial total suction, ψ (MPa)	3.1	4.1
Particle sizes < 40 µm (%)	99.8	97.0
Particle sizes < 2 µm (%)	31.3	55.7
Liquid limit, w_L (%)	134	61.3
Plasticity index, PI (%)	105	38.1

3. Experimental program

3.1. Testing equipment

A new and fully instrumented oedometer setup (Sau 2021) was used to explore the THM behaviour of Ycs. It allows performing isothermal loading-unloading paths at different temperatures and heating-cooling (H-C) cycles at constant vertical stress. The vertical total stress (σ_v) and hydraulic boundary conditions at the top (u_t) and bottom (u_b) caps of the sample are applied using three pressure/volume controllers (PVC) as shown in the schematic in Fig. 1. The heater band (H) encircles the oedometer ring, and the temperature controller (TR) allows programming heating/cooling ramps. The heat loss is minimised using a casing made of high-performance thermoplastic PEEK^{TM} (light grey casing in the schematic).

The main features of this setup are the capability of monitoring the pore water pressure (Pw) and the temperature (T_s) at the bottom of the soil sample and measuring the lateral stresses during loading-unloading and heating-cooling paths. The lateral stress system comprises two high-resolution linear variable differential transformers (LVDTs) orthogonally placed in contact with an Invar ring with reduced thermal expansion and a localised thin wall (LVDT-$H_{1,2}$). The calibration of the deflection of the thin-wall ring at different pressures and without ovaling of the circular section allows for determining the lateral stress. The resolution of the LVDTs (0.24 µm) sets a resolution of 28 kPa for the radial stress. The dimensions of the sample are 50 mm in diameter and 25 mm high.

Cell calibrations related to thermal and mechanical loads are mandatory to interpret experimental data correctly. Particularly crucial is the calibration to estimate radial stresses from the deflection of the ring's wall at different temperatures (Sau 2021).

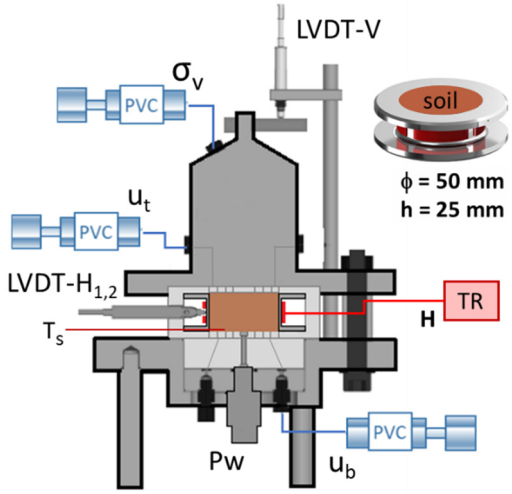

Figure 1. Schematics of oedometer ring with a sample and the thermal oedometer setup with pore pressure transducer (Pw), vertical LVDT-V, horizontal LVDT-H, thermocouple inside the soil sample (T_s), water inlet (u_b) and outlet (u_t), heater band (H), temperature controller (TR) and pressure/volume controllers (PVC) to apply vertical stress (σ_v) and backpressures.

3.2. Testing protocols

Two tests were performed on samples trimmed with bedding planes orthogonal to the axisymmetric axis.

The induced matric suction was considered to define the pre-conditioning stress paths since samples can undergo swelling and possible degradation in contact with water at low stresses (Ferrari and Romero 2019; Sau, Romero, and Van Baelen 2020). Therefore, samples were loaded to vertical total stresses slightly higher than

the *in situ* effective stresses and, only then, placed in contact with synthetically prepared Ycs water (SYCW) at atmospheric pressure and equivalent osmotic suction (around 0.56 MPa). Then, a flow was induced by applying a reduced hydraulic gradient using both backpressure PVCs. Afterwards, a water backpressure of 0.5 MPa was applied at the samples' top and bottom boundaries (u_t and u_b), reaching the same vertical effective stress as the *in situ* one.

Fig. 2 depicts the thermo-mechanical (TM) paths as a function of the vertical effective stress σ_v' and the controlled temperature of the heater (T_{HEATER}), and starting from *in situ* states. Fig. 3 shows an example of an H-C cycle, in which T_{HEATER} increases and decreases in steps of 10°C. The stepwise increase/decrease of T_{HEATER} is well-controlled with a stabilising period of 15 hours to avoid the generation of excess pore water pressure or depressurisation in case of cooling.

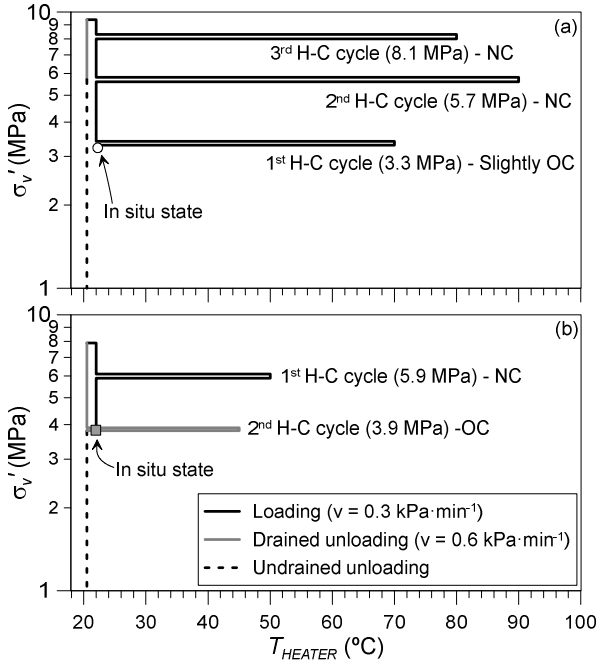

Figure 2. TM paths. (a) Core-48. (b) Core-103.

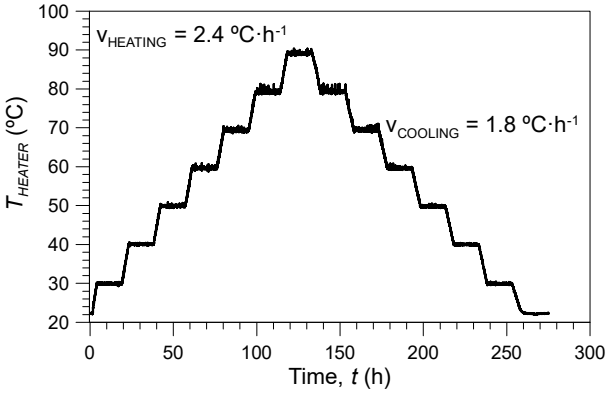

Figure 3. Example of an H-C cycle.

On Core-48, the first heating-cooling H-C cycle was performed at *in situ* stress conditions, i.e. under slightly overconsolidated (OC) conditions (Fig. 2a). After the H-C cycle, the vertical total stress was slowly increased at 0.3 kPa·min^{-1} to avoid pore water pressurisation while the backpressure at the boundary was kept constant. Then, a second H-C cycle was carried out at normally consolidated (NC) conditions (2nd H-C in Fig. 2a). Drained loading was completed to perform a third H-C cycle under NC conditions at a higher stress level (3nd H-C in Fig. 2a). Finally, the unloading was performed in two stages. The first was executed under drained conditions (0.6 kPa·min^{-1}) to evaluate the compressibility parameters. Then, the vertical stress was instantaneously reduced while the top and bottom valves were closed.

Fig. 2b depicts the testing protocol of Core-103. First, the sample was slowly loaded to reach NC conditions. Then, the first H-C cycle was performed (1st H-C in Fig. 2b). Subsequently, the sample was loaded under drained conditions to 7.9 MPa and then unloaded to 3.9 MPa to study the compressibility parameters. Next, the second H-C cycle was performed under OC conditions at *OCR*=2 (2nd H-C in Fig. 2b). Finally, the total vertical stress was instantaneously reduced while the top and bottom valves were kept closed.

4. Results and interpretation

4.1. Pre-conditioning stage

Fig. 4 depicts the evolution of vertical deformation, void ratio and degree of saturation throughout the loading path to *in situ* stress at constant water content. The decrease of the air pore space leads to an increase in saturation. As a result, Core-103 reaches saturation at the

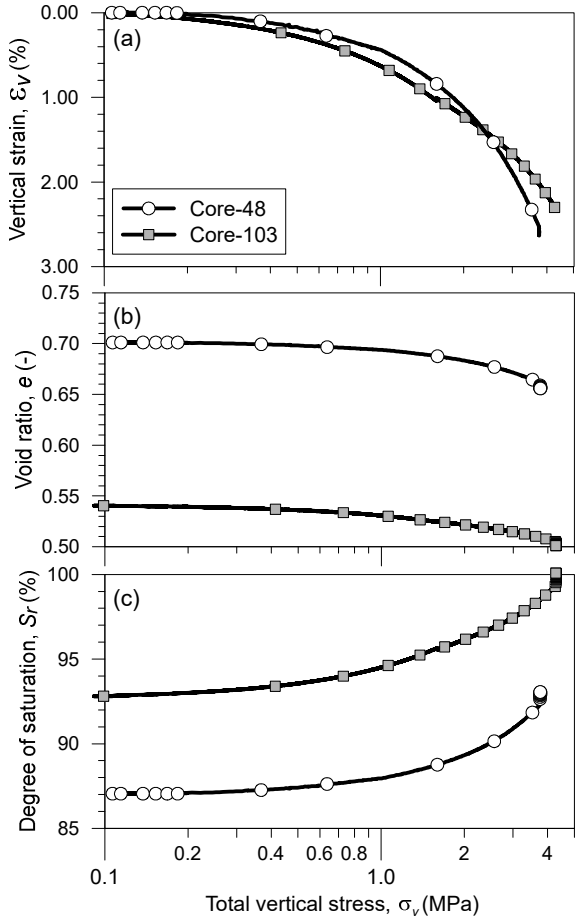

Figure 4. Pre-conditioning stage. Evolution of vertical deformation, void ratio and degree of saturation.

end of the loading path. The compression behaviour in this unsaturated state is associated with the increase in the total stress and the decrease in matric suction due to meniscus curvature changes. Nevertheless, despite reaching saturation, some matric suction may remain as there may still be some meniscus curvature.

The expansion that occurred during soaking with SYCW was relatively small, indicating a reduced remaining matric suction. The maximum values were 0.03 % and 0.06 % for Core-48 and Core-103, respectively.

4.2. Compressibility beyond *in situ* stress state

Fig. 5 depicts the compressibility curves (vertical strain) in terms of the mean effective stress (p'). The variations in p' during H-C cycles arise from changes in radial stresses since the vertical effective stress is kept constant during non-isothermal paths. At a slightly OC state (Core-48), the drained H-C cycle showed a quasi-reversible response in volume changes and radial stresses (refer to section 4.3). At OCR=2 on Core-103, the response was reversible with expansion on drained heating (at least up to T_{max}=45ºC). However, in NC states, the volume change was not reversible with a contractive response on heating and cooling depending on the stress state.

The increase in the elastic domain due to mean effective stress increase (radial stress increase) on drained heating at NC conditions is detected. During the subsequent mechanical loading, there is a clear transition between the elastic and elastoplastic domains, as presented in Fig 5a. Table 2 summarises the pre-yield and post-yield compressibility parameters (change in the void ratio over the change in ln p').

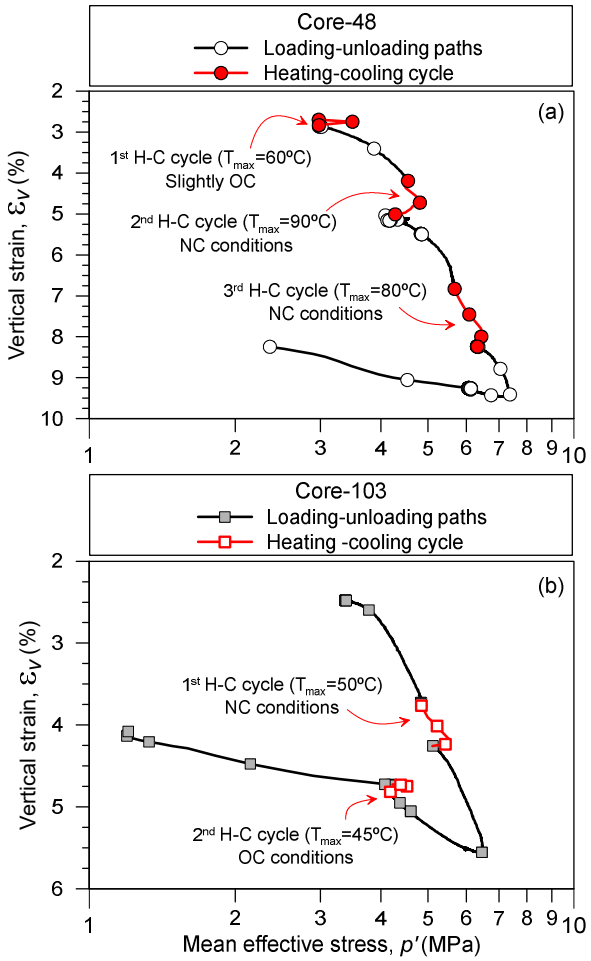

Figure 5. Compressibility curves beyond *in situ* stress: (a) Core-48, (b) Core-103.

Table 2. Pre-yield κ and post-yield λ compressibility parameters.

	λ	κ
Core-48	0.112	0.026
Core-103	0.093	0.021

Samples show time effects in vertical strains (creep) and radial stresses (stress relaxation) at the end of the loading paths, particularly at high stresses. No significant excess pore pressure was measured during the slow loading paths. Concerning the final undrained stage in Core-103, a minor swelling was recorded due to water inflow from the drainage lines to the sample.

Fig. 6 shows the stress paths in a mean effective stress: deviatoric stress (p':q) plane. The loading paths under NC states in Core-103 (Fig. 6b) maintain the initial stress obliquity η_{NC} (dashed green line), even after the H-C cycle at T_{max}=50ºC. This trend is not observed in NC sample Core-48 (Fig. 6a), which deviates from the initial obliquity η_{NC} (dashed green line) after the H-C cycle at T_{max}=90ºC. As observed in the plot, there is a systematic increase of p' and a decrease of q induced on drained heating (associated with the radial stress increase).

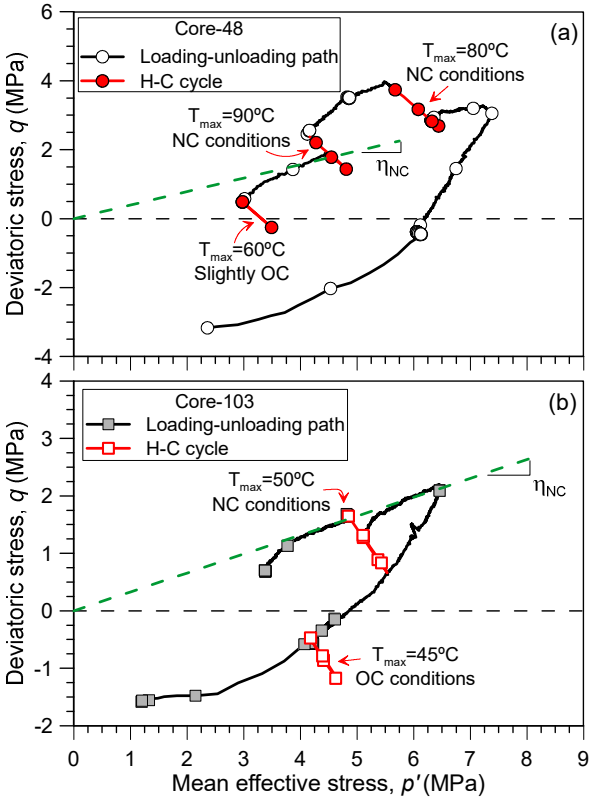

Figure 6. Stress paths in p':q plane: (a) Core-48, (b) Core-103.

4.3. Thermal-induced strains

This section presents the volume changes upon drained H-C cycles at different mean stresses and *OCRs*. Fig. 7 summarises the vertical deformation (dashed lines) and the volumetric deformation (solid lines with symbols) along the drained H-C cycles in Core-48 and Core-103. In addition, volumetric strains are computed considering the small local radial displacements measured at the mid-plane of the thin-wall section of the Invar oedometer ring. Differences between these deformations are mainly associated with radial stress changes and thin-wall deflections on H-C cycles, since ring thermal dilation is very small (0.008% at 90ºC).

As observed, the thermal-induced volumetric behaviour is mostly contractive. The only exception is the response of Core-103 at OC state (*OCR*=2), in which the sample undergoes expansion of 0.1 % after a temperature rise of 20°C. Even the H-C cycle on Core-48 at the slightly OC *in situ* condition (*YSR*≈1.5) shows a small contractive response of around 0.14 %. The measurements during the three H-C cycles of Core 48 show that the irreversible contractive response on heating increases with effective stress. In addition, the three cooling paths indicate contractive deformations that increase with effective stress.

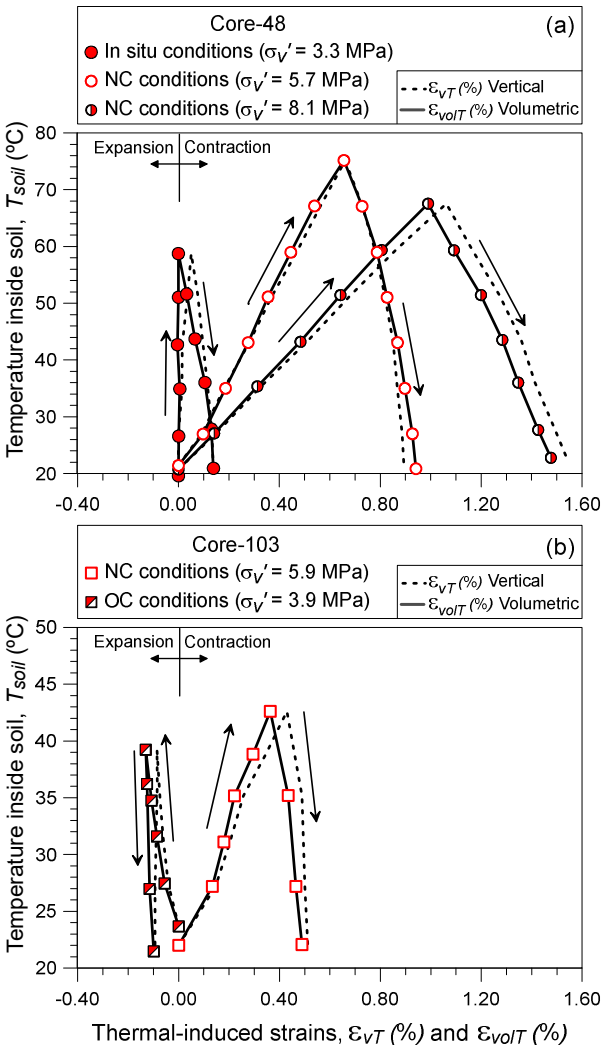

Figure 7. Thermal-induced strains during H-C cycles: (a) Core-48, (b) Core-103.

4.4. Thermo-mechanical elastoplastic interpretation

This section interprets the volume change response of Core-48 within a TM elastoplastic framework. Drained temperature increases results in a reversible expansion (temperature and stress-dependent) of clay skeleton and different soil constituents (minerals and aggregates) and a concurrent irreversible contraction of the porous skeleton, which is dominant in NC states (or at low *OCRs*) and increases with effective stress.

The variation of drained reversible thermal expansion coefficients with temperature and stress state can be described using a similar expression to the one in (Baldi, Hueckel, and Pellegrini 1988), which (Romero 1999) also considered on compacted Boom Clay under isotropic stress states:

$$\left.\frac{\delta\varepsilon_{vT}^{e}}{\delta T}\right|_{p'} = \alpha(\Delta T, p') = \alpha_m + \alpha_0(p') + \alpha_1(p')\Delta T \qquad (1)$$

$$\text{with } \alpha_i(p') = \alpha_i^a + \alpha_i^b \ln\frac{p'}{p'_r}$$

where ΔT is the temperature difference to the initial temperature (≈22°C), and p'_r = 0.01 MPa a reference mean effective stress. The drained reversible thermal expansion coefficient $\alpha(\Delta T,p')$ includes the thermal expansion coefficient of the solid constituents α_m, which is assumed to be independent of stress, and that of the porous skeleton (α - α_m) dependent on stress state and temperature. The parameters that describe such dependence are α_0^a, α_0^b, α_1^a and α_1^b. As a weighted average, the coefficient α_m was estimated based on the mineralogical composition and thermal expansion coefficients of forming minerals. The coefficients $\alpha(\Delta T,p')$ were determined from the slopes of the cooling paths at different mean stresses.

Fig. 8 shows the variation of $\alpha(\Delta T,p')$ with ΔT at varying average mean effective stresses. Fig. 9 complements the information by presenting the changes of $\alpha(\Delta T,p')$ at different average p' and classified for several ΔT. As observed, there is no significant effect of the stress state between 3 and 4.5 MPa, particularly at low ΔT. On the contrary, there is a clear effect of the stress state at higher p' (above 4.5 MPa). A least-squares algorithm using all reported data allow for determining the drained thermal expansion coefficients of Eq. (1), which are reported in Table 3.

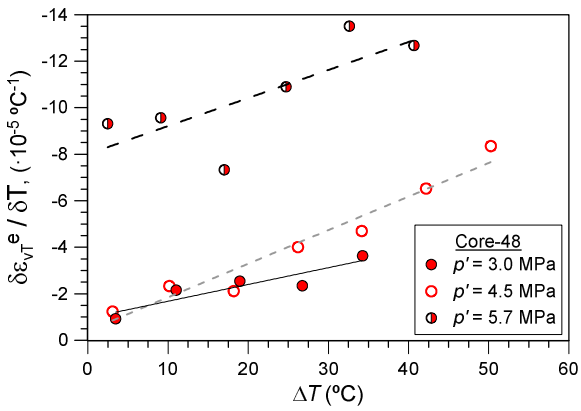

Figure 8. Temperature dependence of $\alpha(\Delta T,p')$.

Table 3. Drained thermal expansion coefficients of particles and porous skeleton.

	α_m	$\alpha_0{}^a$	$\alpha_0{}^b$	$\alpha_1{}^a$	$\alpha_1{}^b$
	$\times 10^{-5}$ °C^{-1}				
Core-48	-2.27	48.9	-8.1	0.8	-0.15

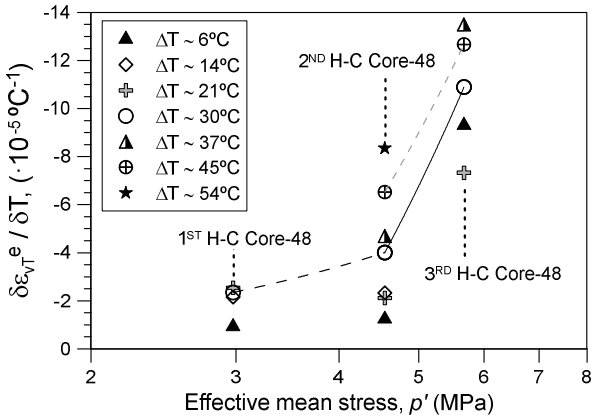

Figure 9. Stress dependence of $\alpha(\Delta T,p')$.

The irreversible and contractive volume change response of NC states on drained heating at approximately constant p' is associated with volumetric strain-hardening effects to compensate for the shrinkage of the thermoelastic domain (thermal softening). Therefore, the drained irreversible thermal coefficients $\frac{d\varepsilon_{vT}^{p}}{dT}$ can be used to determine the uncoupled thermal softening function of the yield locus $A(\Delta T)$. Several expressions are proposed to describe the thermal softening function, for instance (Laloui and Cekerevac 2003). However, the present study uses a straightforward expression proposed by (Hueckel and Baldi 1990), which was also considered by (Romero 1999) due to its uncoupled character on compacted Boom Clay under isotropic stress states:

$$A(\Delta T) = a_1 \Delta T + a_2 \Delta T^2 \tag{2}$$

where a_1 and a_2 are the coefficients of thermal sensitivity of the yield surface, and ΔT the temperature difference. The following yield stress p'_c keeps uncoupled the thermal and volumetric plastic strain dependence:

$$p'_c\,(\varepsilon_v^P, \Delta T) = p'_0(\varepsilon_v^P) + A(\Delta T) \tag{3}$$

where $p'_0\,(\varepsilon_v{}^P)$ is the Cam-Clay hardening parameter that depends only on plastic volumetric strains $\varepsilon_v{}^P$ (κ and λ are the pre-yield and post-yield compressibility parameters in Table 2, and e_0 is the void ratio before the heating path):

$$\delta p'_0 = \frac{(1+e_0)p'_0}{(\lambda-\kappa)}\,\delta\varepsilon_v^P \tag{4}$$

Thus, for the consistency condition during drained heating -temperature increment δT- at constant stress state at yielding (f represents the yield surface):

$$\frac{\partial f}{\partial T}\delta T + \frac{\partial f}{\partial \varepsilon_v^P}\delta\varepsilon_v^P = 0 \tag{7}$$

The above expression transforms to:

$$\frac{\delta\varepsilon_{vT}^P}{\delta T} = \frac{-\partial p'_c/_{\partial T}}{\partial p'_c/_{\partial \varepsilon_v^P}} = \frac{-(\lambda-\kappa)(a_1+2a_2\Delta T)}{(1+e_0)p'_0} \tag{8}$$

Fig. 10 depicts the irreversible (contractive) thermal coefficients against temperature increment. The linear interpolations and the initial values before each H-C cycle allow for determining the coefficients of the thermal softening function for each stress level (summarised in Table 4). These values for Ycs will be compared with compacted Boom Clay results reported by (Romero 1999) in section 5.

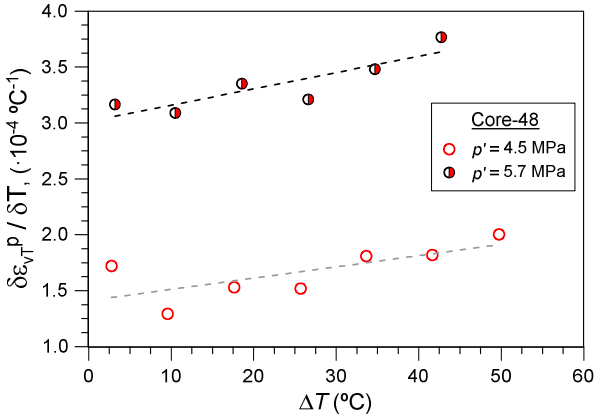

Figure 10. Drained irreversible thermal coefficients against temperature increment.

Table 4. Coefficients of thermal sensitivity of the yield surface (NC states).

	p'_0	e_0	a_1	a_2
	MPa	-	**MPa°C^{-1}**	**MPa°C^{-2}**
Core-48	4.5	0.60	$-1.2\cdot10^{-2}$	$-4.2\cdot10^{-5}$
	5.7	0.56	$-3.1\cdot10^{-2}$	$-7.7\cdot10^{-5}$

5. Summary and discussion

This paper explores the THM behaviour of Ycs using experimental results obtained with a newly designed and fully instrumented oedometer cell with lateral stress measurement. First, tests focus on restoring equivalent *in situ* vertical stresses before placing samples in contact with synthetic water of the formation, which effectively avoided their swelling on remaining matric suction reduction. Then, experimental efforts aim at characterising the evolution of radial stresses and the volume change response on loading/unloading. Finally, these stress paths allow targeting different *OCRs* and mean effective stresses before performing the main research goal of drained H-C cycles at varying stress histories and states.

The nature of the thermal-induced volume changes in Ycs is in line with the behaviour observed on other plastic argillaceous formations. Drained heating at NC conditions causes irreversible contraction, and at OC, the soil expands as long as the maximum temperature does not reach a certain threshold. (Delage, Sultan, and Cui 2000; Sultan, Delage, and Cui 2002; Yu et al. 2018) have

observed in Boom Clay that drained heating at OC conditions and high temperatures induces an initial expansive response followed by contractive behaviour, whose transition temperature increases with increasing *OCRs*. (Yu et al. 2018) have reported that the threshold temperature for Boom Clay at *OCR*=2 is 50ºC. In the current study, the H-C cycle at the slightly OC *in situ* condition shows a small contractive response at $T > 42$ºC, whereas the Ycs sample at *OCR*=2 and heated to 40ºC does not undergo any irreversible contraction. At these OC states, radial stresses on an H-C cycle display a quasi-reversible response (radial stress increase in drained heating and equivalent decrease in cooling). In addition, the irreversible contractive response of Ycs at NC states depends on the stress state (more significant contractions at higher mean effective stresses). This observation differs from (Sultan, Delage, and Cui 2002) on NC Boom Clay, who have assumed that thermal-induced plastic contraction is independent of the mean effective stress applied. In addition, at NC conditions and constant vertical effective stress, there is an irreversible change in radial stresses in an H-C cycle, which induces mean effective stress to increase (radial stress increase). During the subsequent mechanical loading after the H-C cycle, there is an increase in the elastic domain detected by a clear transition between the elastic and elastoplastic domains.

The paper also interprets thermal-induced volume changes within a TM elastoplastic framework. Reversible and irreversible volume change responses show dependence on temperature, stress state and history. Thermal expansion (reversible) coefficients have been fitted to a well-known expression as a function of temperature increment and stress state. A simplified procedure is also presented to define the thermal sensitivity coefficients, a_1 and a_2, of a well-known uncoupled thermal softening function from plastic volumetric strains. The coefficients depend on the mean effective stress, which should be incorporated in future refinements of this function. The thermal sensitivity coefficient a_1=-1.5×10^{-2} MPaºC^{-1} reported by (Romero 1999) for NC Boom Clay at mean effective stress of 1 MPa and e_0=0.68 is in the same range as the ones presented in Table 4. The same author reported a positive value of the thermal coefficient a_2=6.3·10^{-5} MPaºC^{-2} for Boom Clay (remaining the thermal softening function always negative), which could help better define the coefficient's dependence on the stress state with the data in Table 4.

Acknowledgements

The authors are grateful for the financial support provided by 'Organisme National des Déchets Radioactifs et des Matières Fissiles Enrichies' ONDRAF/NIRAS (Belgium) through a PhD collaboration agreement with the 'International Centre for Numerical Methods in Engineering' CIMNE (Spain) within the context of the Project 'Thermal aspects and their coupled HM effects on Ypresian clays and Boom Clay' CCHO 2016-0206/00/02 and CCHO 2019-0236/00/00.

References

Baldi, G., T. Hueckel, and R. Pellegrini. 1988. "Thermal Volume Change of Mineral Water System in Low Porosity Clay." *Can. Geotech. J.*.

Delage, P., N. Sultan, and Y.J. Cui. 2000. "On the Thermal Consolidation of Boom Clay." *Can. Geotech. J.* 37 (2): 343–54. https://doi.org/10.1139/t99-105.

Ferrari, A., and E. Romero. 2019. "In Shale: Subsurface Science and Engineering." *Geophysical Monograph Series, American Geophysical Union*.

Hueckel, T., and G. Baldi. 1990. "Thermoplasticity of Saturated Clays: Experimental Constitutive Study." *Journal of Geotech. and Geoenviron. Eng. ASCE* 116 (12): 1778–96.

Hueckel, T., and M. Borsetto. 1990. "Thermoplasticity of Saturated Soils and Shales: Constitutive Equations." *J. of Geotech. Eng.* 116 (12): 1765–77. https://doi.org/10.1061/(ASCE)0733-9410(1990)116:12(1765).

Laloui, L., and C. Cekerevac. 2003. "Thermo-Plasticity of Clays: An Isotropic Yield Mechanism." *Comput. Geotech.* 30 (8): 649–60. https://doi.org/10.1016/J.COMPGEO.2003.09.001.

Lima, A. 2011. "Thermo-Hydro-Mechanical Behaviour of Two Belgian Clay Formations: Boom and Ypresian Clays." Universitat Politècnica de Catalunya, Barcelona.

Loveridge, F., J.S. McCartney, G.A. Narsilio, and M. Sanchez. 2020. "Energy Geostructures: A Review of Analysis Approaches, in Situ Testing and Model Scale Experiments." *Geomech. Energy Environ.* 22 (6): 100173. https://doi.org/10.1016/j.gete.2019.100173.

Nguyen, X. P., Y. J. Cui, A. M. Tang, X. L. Li, and L. Wouters. 2014. "Physical and Microstructural Impacts on the Hydro-Mechanical Behaviour of Ypresian Clays." *Appl. Clay Sci.* 102: 172–85. https://doi.org/10.1016/j.clay.2014.09.038.

Romero, E. 1999. "Characterisation and Thermo-Hydro-Mechanical Behaviour of Unsaturated Boom Clay: An Experimental Study." Universitat Politècnica de Catalunya.http://www.tdcat.cesca.es/TDCat-0930102-092135/.

Romero, E., N. Sau, A. Lima, H. Van Baelen, X. Sillen, and X. Li. 2016. "Studying the Thermal Conductivity of a Deep Eocene Clay Formation: Direct Measurements vs Back-Analysis Results." *Geomech. Energy Environ.* 8: 62–75.https://doi.org/10.1016/j.gete.2016.10.005.

Sau, N. 2021. "Thermo-Hydro-Mechanical Behaviour of a Deep Argillaceous Formation." Universitat Politècnica de Catalunya, Barcelona. http://hdl.handle.net/10803/687821

Sau, N., E. Romero, and H. Van Baelen. 2020. "Restoring Initial Conditions in a Deep Argillaceous Formation with Induced Suction on Retrieval." *E3S Web of Conferences* 195. https://doi.org/10.1051/e3sconf/202019504012.

Sultan, N., P. Delage, and Y. J. Cui. 2002. "Temperature Effects on the Volume Change Behaviour of Boom Clay." *Eng. Geol.* 64 (2–3): 135–45. https://doi.org/10.1016/S0013-7952(01)00143-0

Yu, H., W. Chen, Z. Gong, Y. Ma, G. Chen, and X. Li. 2018. "Influence of Temperature on the Hydro-Mechanical Behavior of Boom Clay." *Int. J. Rock Mech. Min. Sci.* 108 (July): 189–97. https://doi.org/10.1016/j.ijrmms.2018.04.023